Applied Surface Science 456 (2018) 124–132

Contents lists available at ScienceDirect

Applied Surface Science

journal homepage: www.elsevier.com/locate/apsusc

Full Length Article

# Comparison of performance and optoelectronic processes in ZnO and $TiO_2$ nanorod array-based hybrid solar cells

Fan Wu[a,b,*], Qiquan Qiao[b], Behzad Bahrami[b], Ke Chen[b], Rajesh Pathak[b], Sally Mabrouk[b], Yanhua Tong[c], Xiaoyi Li[a], Tiansheng Zhang[a], Ronghua Jian[a]

[a] School of Sciences and Key Lab of Optoelectronic Materials and Devices, Huzhou University, Huzhou 313000, China
[b] Center for Advanced Photovoltaics, Department of Electrical Engineering and Computer Sciences, South Dakota State University, Brookings, SD 57007, United States
[c] Department of Materials Chemistry, Huzhou University, Huzhou 313000, China

ARTICLE INFO

*Keywords:*
Solar cells
Hybrid semiconductor
Optoelectronic processes
Nanorod array

ABSTRACT

The reported efficiencies of pristine ZnO nanorod array (NRA)-based polymer-inorganic hybrid solar cells (HSCs) are normally lower than those of their pristine $TiO_2$ NRA-based counterparts. This difference typically results from the lower short-circuit current density ($J_{sc}$) of the ZnO NRA device. This paper presents a comparative study of pristine ZnO and $TiO_2$ NRA-based HSCs. We investigate the morphological structure (length, diameter, number density, area of nanorod laterals), photovoltaic performance (current density-voltage *J–V*, external quantum efficiency EQE), and optoelectronic processes related to electron transfer (electron mobility $\mu_e$, electron diffusion length $L_D$, electron lifetime $\tau_e$ and electron transit time $\tau_t$ related electron collecting efficiency $\eta_{cc}$, electron injection $\eta_{inj}$, surface potential SP, photoluminescence PL, bound charge pairs BCP) in HSCs, with ZnO and $TiO_2$ NRA as electron acceptor. Our comparative investigations reveal that the factors relating to the interface area, $\mu_e$, $L_D$, and $\eta_{cc}$ are not the key factors responsible for the difference in the value of $J_{sc}$ in ZnO and $TiO_2$ NRA-based HSCs with the same device structure. In fact, the crucial step for a lower $J_{sc}$ in ZnO NRA-based HSCs than in $TiO_2$ NRA-based HSCs is attributed to the less efficient transfer of photo-generated electrons at the charge separation interface in ZnO NRA-based HSCs. Dynamic characterizations indicate that the transfer of interfacial photo-generated electrons in $TiO_2$ NRA-based HSCs is more efficient than ZnO NRA-based HSCs, and is confirmed by Kelvin probe force microscopy (KPFM) and PL studies. The reason for the better interface charge transfer property in MEH-PPV/$TiO_2$ NRA than that of in MEH-PPV/ZnO NRA is further investigated by Marcus model, we find that more trapped BCP states are generated in the ZnO NRA based HSCs, which resulting in lower interfacial electron injection efficiency from polymer to ZnO NRA.

## 1. Introduction

Polymer-inorganic hybrid solar cells (HSCs) based on a conjugated polymer as the donor (D) and inorganic semiconductor nanocrystals as the acceptor (A) in a bulk heterojunction structure are interesting and promising for photovoltaic energy conversion owing to their advantages of being low-cost, simple fabrication by processing from solution, and the fact that they can be used to fabricate flexible devices [1,2]. A material comprising a combination of ZnO and $TiO_2$ is attractive for nanoscale optoelectronic devices, because it is a wide band gap semiconductor with good carrier mobility [3]. A promising photovoltaic device architecture consisting of direct and ordered electron transport pathways formed by an ZnO and $TiO_2$ nanorod array (NRA) instead of the disordered channels provided by nanoparticles has been proposed [4,5], as shown in Fig. 1.

The band gap of ZnO is similar to that of $TiO_2$, and the conduction band edge of both materials is located at approximately the same level [3–5]. However, the electron mobility exhibited by ZnO NRA is orders of magnitudes higher than that of $TiO_2$ NRA [6–8], which suggests that ZnO NRA-based HSCs should have superior performance. Table 1 lists some performance properties recently reported for pristine ZnO and $TiO_2$ NRA-based HSCs without any interfacial modification or fullerene incorporated in the polymer. Interestingly, most of the efficiencies reported for the pristine ZnO NRA-based solar cells (0.02–0.76%) [9–20] are normally lower than those of pristine $TiO_2$ NRA-based solar cells (0.21–1.74%) [21–29], which is generally a consequence of the higher short-circuit current density $J_{sc}$ in a $TiO_2$ NRA device (1.47–5.15 mA/cm$^2$) compared to its pristine ZnO NRA counterpart (0.52–3.20 mA/cm$^2$).

In fact, a similar phenomenon has also been observed in dye-

* Corresponding author at: School of Sciences and Key Lab of Optoelectronic Materials and Devices, Huzhou University, Huzhou 313000, China.
*E-mail address:* wufan@zjhu.edu.cn (F. Wu).

https://doi.org/10.1016/j.apsusc.2018.06.097
Received 2 March 2018; Received in revised form 20 May 2018; Accepted 12 June 2018

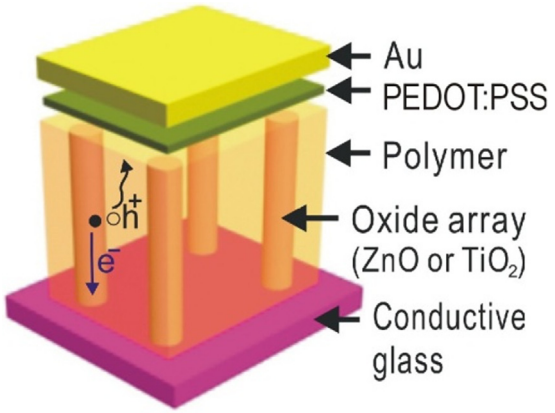


**Fig. 1.** Architecture of polymer/oxide array HSCs. The arrows show the electron ($e^-$, solid point) and hole ($h^+$, empty circle) transportation.

**Table 1**
Recently reported performance of HSCs based on pristine ZnO and $TiO_2$ NRA without any interfacial modification or fullerene incorporated in the polymer.

| | Polymer | Year | $V_{oc}$ (V) | $J_{sc}$ (mA/cm$^2$) | FF | PCE (%) | Ref |
|---|---|---|---|---|---|---|---|
| ZnO NRA | P3HT | 2011 | 0.54 | 2.67 | 0.53 | 0.76 | [9] |
| | P3HT | 2012 | 0.37 | 3.19 | 0.41 | 0.48 | [10] |
| | MEH-PPV | 2013 | 0.36 | 1.22 | 0.33 | 0.15 | [11] |
| | P3HT | 2013 | 0.32 | 0.66 | 0.53 | 0.11 | [12] |
| | P3HT | 2013 | 0.32 | 3.20 | 0.53 | 0.54 | [13] |
| | P3HT | 2014 | 0.41 | 1.02 | 0.35 | 0.15 | [14] |
| | P3HT | 2015 | 0.26 | 1.41 | 0.41 | 0.10 | [15] |
| | MEH-PPV | 2015 | 0.35 | 1.48 | 0.33 | 0.17 | [16] |
| | P3HT | 2016 | 0.42 | 0.75 | 0.49 | 0.16 | [17] |
| | P3HT | 2016 | 0.38 | 0.86 | 0.33 | 0.11 | [18] |
| | P3HT | 2017 | 0.30 | 1.11 | 0.42 | 0.14 | [19] |
| | P3HT | 2018 | 0.11 | 0.52 | 0.28 | 0.02 | [20] |
| $TiO_2$ NRA | P3HT | 2008 | 0.32 | 3.89 | 0.41 | 0.51 | [21] |
| | P3HT | 2012 | 0.40 | 2.01 | 0.55 | 0.43 | [22] |
| | P3HT | 2013 | 0.39 | 1.47 | 0.38 | 0.22 | [23] |
| | P3HT | 2013 | 0.36 | 2.18 | 0.38 | 0.30 | [24] |
| | MEH-PPV | 2014 | 0.34 | 3.48 | 0.33 | 0.39 | [25] |
| | P3HT | 2015 | 0.65 | 5.15 | 0.52 | 1.74 | [26] |
| | MEH-PPV | 2015 | 0.38 | 2.19 | 0.33 | 0.27 | [27] |
| | P3HT | 2016 | 0.33 | 1.66 | 0.39 | 0.21 | [28] |
| | PCPDTBT | 2017 | 0.62 | 4.10 | 0.43 | 1.10 | [29] |

sensitized solar cells (DSCs), and the lower photocurrent of ZnO NRA-based DSCs has been ascribed to the partial dissolution of the ZnO surface and formation of dye aggregates [30,31]. However, the interface destruction and dye aggregates do not exist in HSCs because of the use of moderated conjugated polymer instead of dye. Therefore, it needs to be clear which processes are responsible for the weaker photocurrent in ZnO NRA-based HSCs compared to their $TiO_2$ NRA counterparts. To the best of our knowledge, a study involving a one-to-one comparison of the electron transfer properties of ZnO and $TiO_2$ NRA-based HSCs to demonstrate that $TiO_2$ is a superior acceptor for HSCs has not yet been reported. Although the ZnO-$TiO_2$ core-shell structure array has been studied in HSCs and DSCs [3,32,33], it could not readily be concluded that $TiO_2$ NRA is a more effective acceptor than ZnO NRA in HSCs. Because they ascribed the improved performance mostly to the passivation of defect states on the ZnO NRA surface and the modified charge separation interface [32,33], rather than the intrinsic property of $TiO_2$ itself; moreover, the ZnO-ZnO core-shell structure array has also been shown capable of being much more efficient than its pristine ZnO NRA counterpart [34]. Therefore, the ZnO-$TiO_2$ core-shell study does not provide a credible comparison of the transport properties in pristine ZnO and $TiO_2$ NRA in HSCs, which are not yet fully understood. The aim of this study is to compare the performance of HSCs fabricated with pristine ZnO and $TiO_2$ NRA with the aim of identifying the key electronic process responsible for the observed $J_{sc}$ differences in ZnO and $TiO_2$ NRA-based HSCs under illumination, such that strategies for the relative improvement of the device can be formulated.

## 2. Material and methods

### 2.1. Synthesis of ZnO NRA and $TiO_2$ NRA

The ZnO NRA was grown by firstly coating a dense ZnO layer onto patterned fluoride-doped tin oxide (FTO) glass (14 Ω/sq, Huanan Xiangcheng Hi-Tech Co., Ltd., China) by spin-coating (1500 rpm, 60 s) the ZnO precursor solution of zinc acetate (0.327 g) and acetic acid (0.20 mL) in the mixture of 8 mL of anhydrous alcohol and 2 mL of water. The ZnO-NRA was hydrothermally grown by suspending the ZnO-coated FTO conducting glass upside down in an aqueous solution of zinc nitrate hexahydrate (0.025 M) and hexamethylenetetramine (0.025 M) at 90 °C for 2 h in an electric oven to produce the ZnO NRA [34–36].

The $TiO_2$ NRA was hydrothermally grown on FTO-coated glass, following an approach similar to previous work [25,37]. Deionized water was mixed with concentrated hydrochloric acid (35%) (volume ratio:1:1) to reach a total volume of 60 mL in a Teflon-lined stainless steel autoclave (100 mL volume). The mixture was stirred in ambient conditions for 5 min before adding into the Teflon liner, after which the cleaned FTO substrate was inserted upside down in the Teflon liner with the above mixture solution, and 1 mL of titanium (IV) isopropoxide (TTIP, 97%) was added. After 10 min of sonication, the autoclave was sealed and heated at 180 °C for 100 min in an electric oven to produce the $TiO_2$ NRA.

### 2.2. Device fabrication

MEH-PPV (average Mn = 40,000–70,000, Aldrich) and poly(3,4-ethylene dioxythiophene):poly(styrene-sulfonate) (PEDOT:PSS) (Clevios P HC V4, H. C. Starck) were commercially obtained. The MEH-PPV layer was deposited on top of the oxide array by spin-coating (1000 rpm, 40 s) the MEH-PPV solution in chlorobenzene (10 mg/mL) under ambient conditions. This was followed by annealing at 150 °C under $N_2$ atmosphere for 10 min. Subsequently, a PEDOT:PSS film was spin-coated (2000 rpm, 60 s) over the polymer layer. After the deposition of the PEDOT:PSS, the sample was sequentially heated for 10 min at 100 °C in a glove box ($N_2$). Finally, a gold electrode (100 nm) was evaporated through a shadow mask to form an overlapped area of 0.12 cm$^2$ between the FTO and Au, which defined the effective device area.

### 2.3. Characterization and instruments

Scanning electron microscopy (SEM) measurements of the nanostructures, in the form of field-emission scanning electron microscopy (FE-SEM, FEI Sirion200), were carried out. The room-temperature photoluminescence (PL) properties were measured under ambient conditions. PL measurements were performed on a Hitachi F-7000 spectrofluorophotometer. The absorption spectra were recorded with a Shimadzu UV-2600 spectrophotometer. The steady-state *J–V* curves were measured with AM1.5 illumination under ambient conditions using a 94023A Oriel Sol3A solar simulator (Newport Stratford, Inc.) with a 450-W xenon lamp as the light source. Incident photon-to-current efficiency (IPCE) spectra of the solar cells were measured by using a QE/IPCE measurement kit (Zolix Instruments Co., Ltd.) in the spectral range of 300–900 nm. Intensity modulated photocurrent spectra (IMPS) and Intensity modulated photovoltage spectra (IMVS) spectra were characterized by a controlled intensity modulated photo spectroscopy (CIMPS) (Zahner Co., Germany) in ambient conditions with a blue light emitting diode (LED) as illumination source (background illuminating light intensity is 15.85 mW/cm$^2$, and the depth of small sinusoidal